Supplemental Data

Disruption of a Ciliary B9 Protein Complex

Causes Meckel Syndrome

William E. Dowdle, Jon F. Robinson, Andreas Kneist, M. Salomé Sirerol-Piquer, Suzanna G.M. Frints, Kevin C. Corbit, Norran A. Zaghloul, Gesina van Lijnschoten, Leon Mulders, Dideke E. Verver, Klaus Zerres, Randall R. Reed, Tania Attié-Bitach, Colin A. Johnson, José Manuel García-Verdugo, Nicholas Katsanis, Carsten Bergmann, and Jeremy F. Reiter
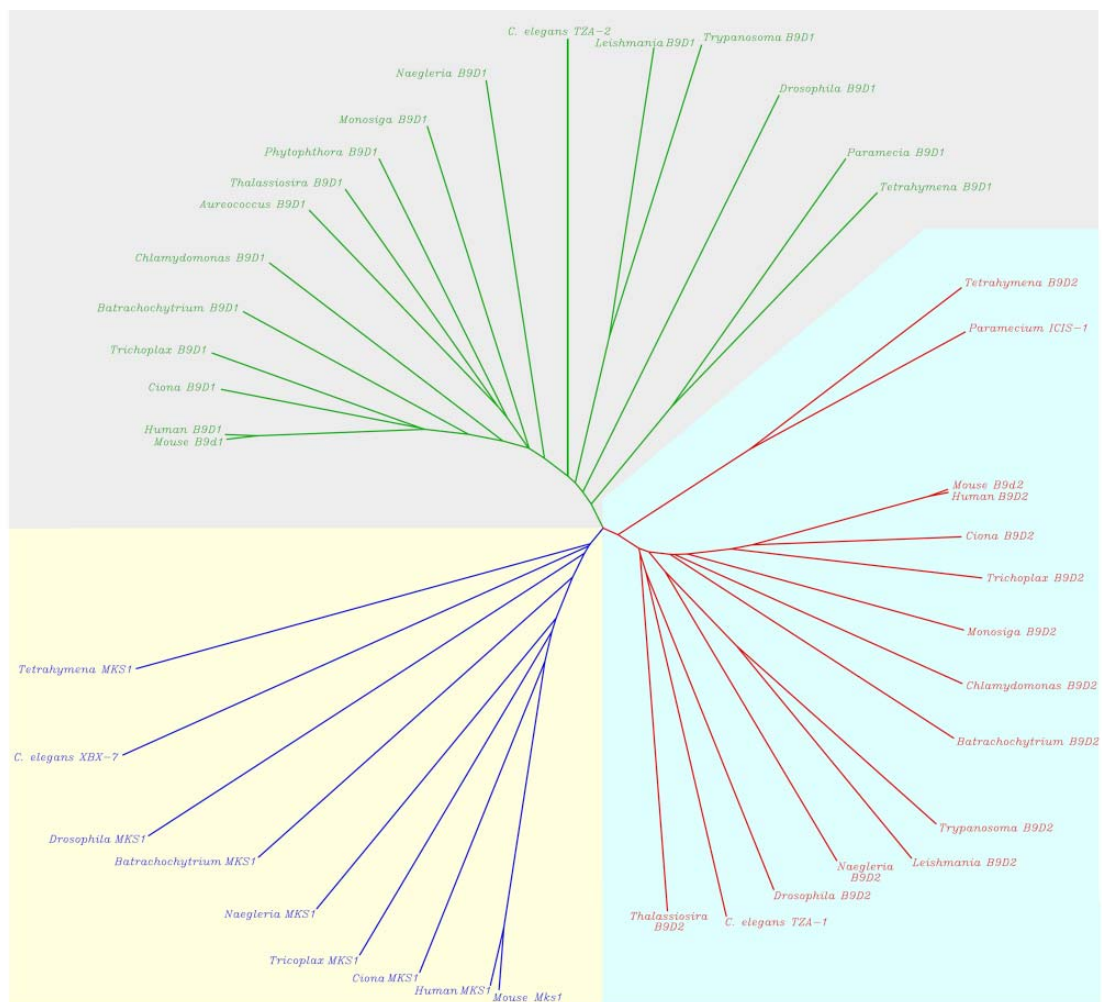

Figure S1. Evolutionary conservation of B9 proteins. Phylogenetic tree of B9 proteins demonstrates conservation of *MKS1, B9D1,* and *B9D2* in diverse ciliated organisms.
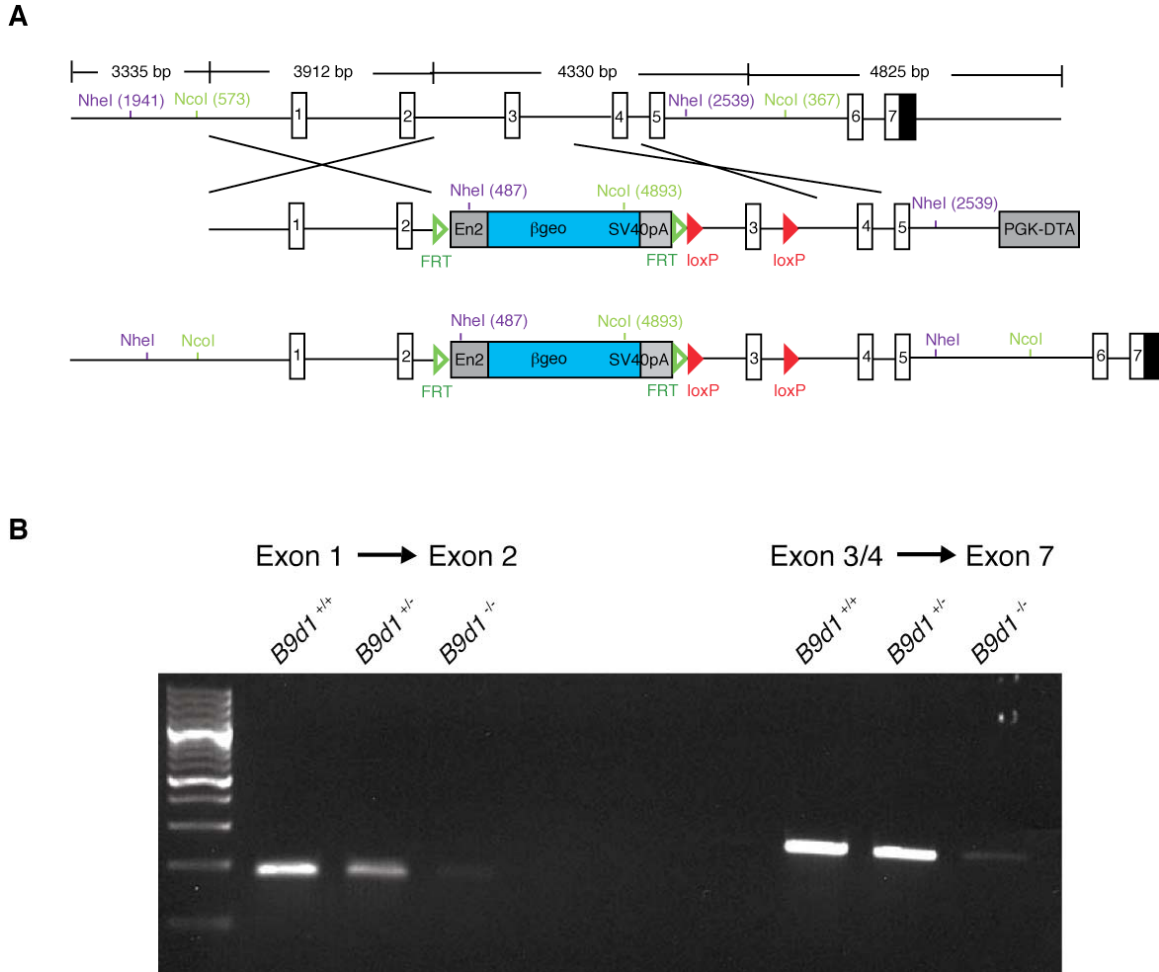
Figure S2. *B9d1^tm1a(EUCOMM)Wtsi* **is a strong hypomorphic or null allele. (A)** Schematic of the targeting strategy to generate *B9d1^tm1a(EUCOMM)Wtsi*. A splice acceptor of an *Engrailed2* intron (En2) generates a fusion between the first 44 amino acids of *B9d1* and a βgeo reporter. **(B)** RT-PCR of E9.5 embryo mRNA utilizing two separate primer pairs, with a sense primer homologous to a region of exon 1 and an antisense primer homologous to a region of exon 2 (left), or a sense primer homologous to a region spanning exon 3 and 4 and an antisense primer homologous to a region within exon 7 (right), revealing that *B9d1* mRNA is strongly reduced in embryos homozygous for the *B9d1* mutation.
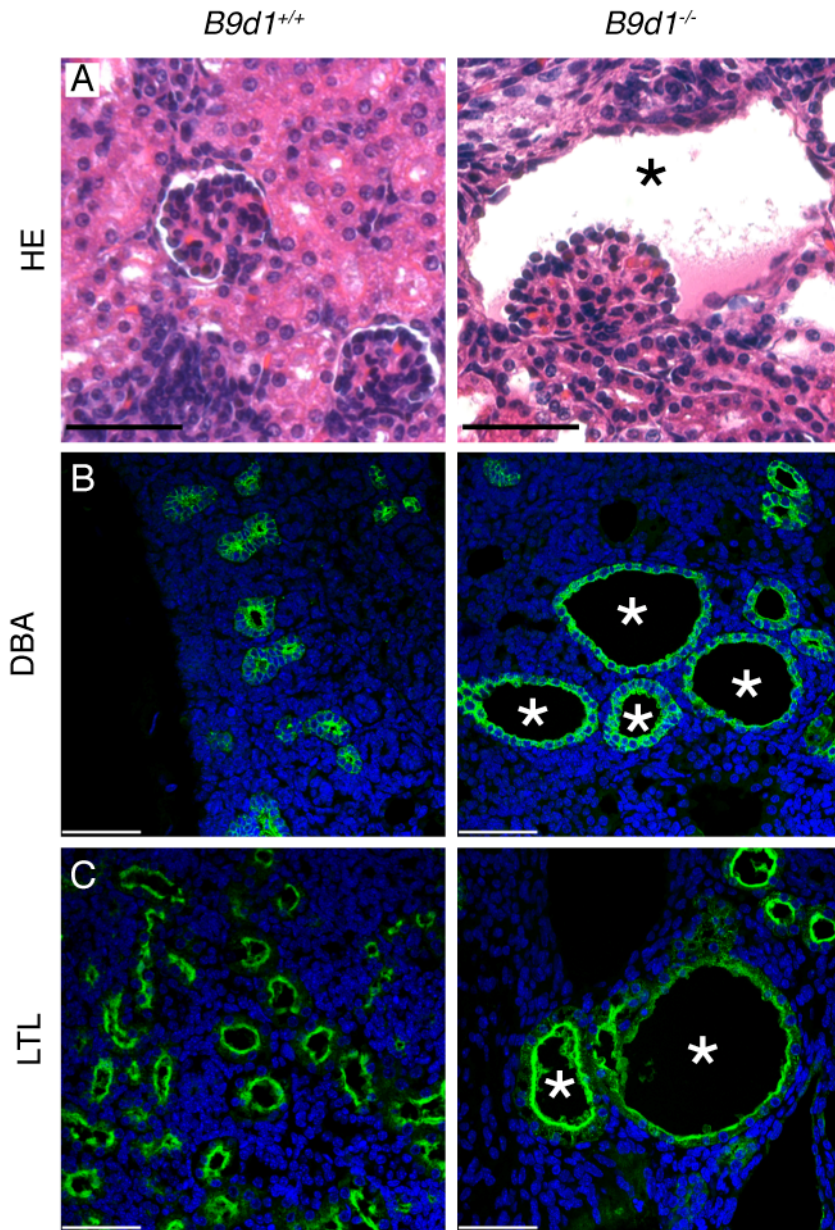
Figure S3. Multiple origins of *B9d1* mutant renal dilations and cystic lesions. (A) Hematoxylin and eosin-stained coronal section of P1 kidneys shows dilation of the Bowman's capsule (asterisk) surrounding the glomerulus in a *B9d1* mutant kidney. Scale bar, 50μm. **(B)** Kidney sections stained with a marker of collecting ducts (*Dolichous biflorus* lectin (DBA), green) and nuclei (DAPI, blue) or **(C)** a marker of proximal tubules (*Lotus tetragonolobus* lecting (LTL), green) and nuclei (DAPI, blue). **(B-C)** Large cysts (asterisks) are found in both regions of the *B9d1* mutant kidneys. Scale bar, 50μm.
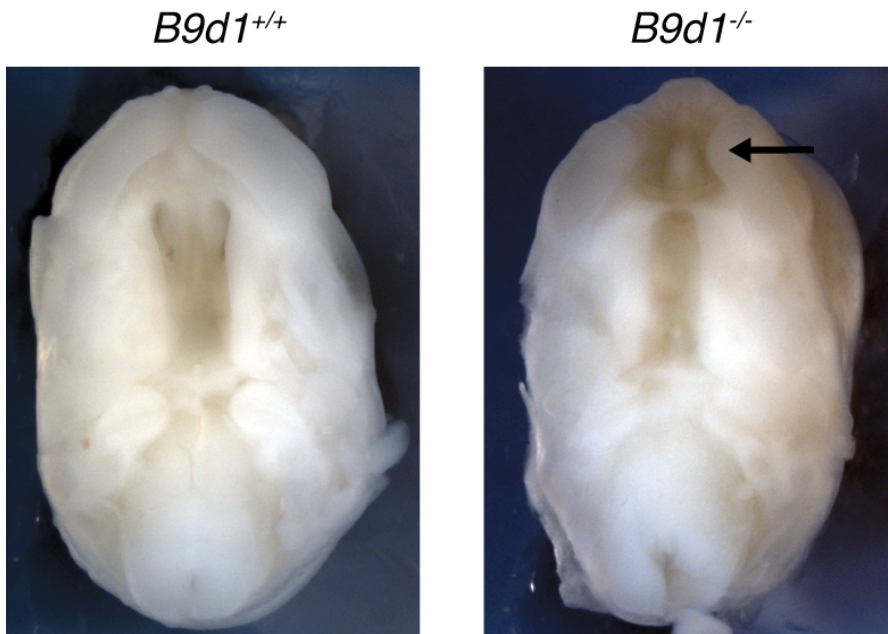
Figure S4. *B9d1* mutants develop cleft palate. Ventral view of E13.5 embryo palates reveals clefting of the primary palate (lip) in *B9d1* mutants (arrow).
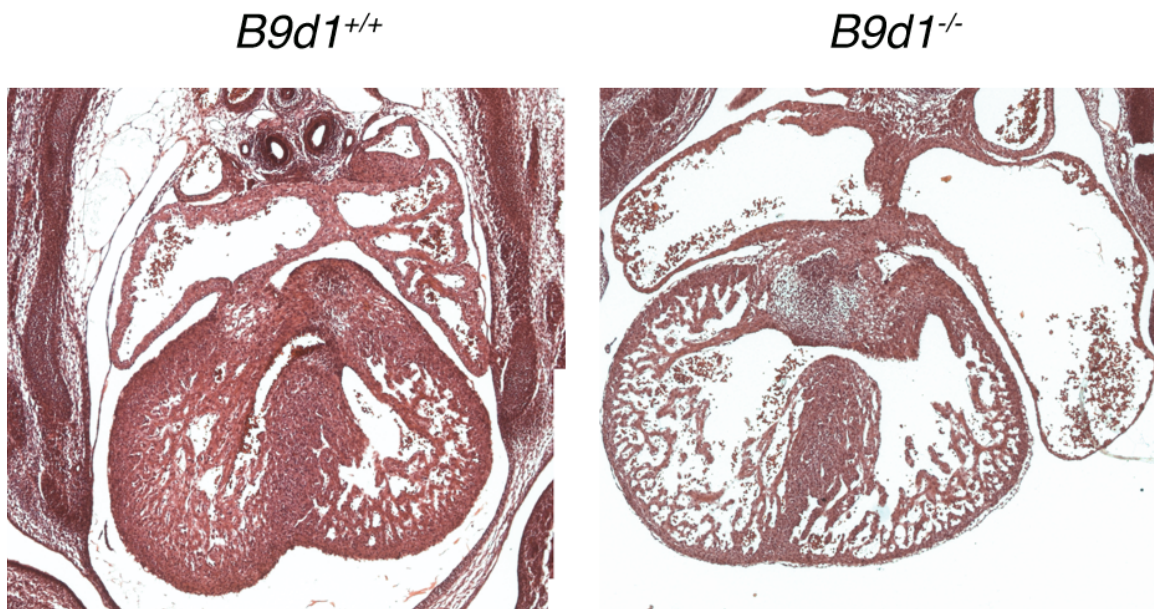

Figure S5. *B9d1* mutants display ventricular septal defect. H&E stained transverse section of E13.5 hearts. *B9d1* mutants fail to complete the membranous ventricular septum.
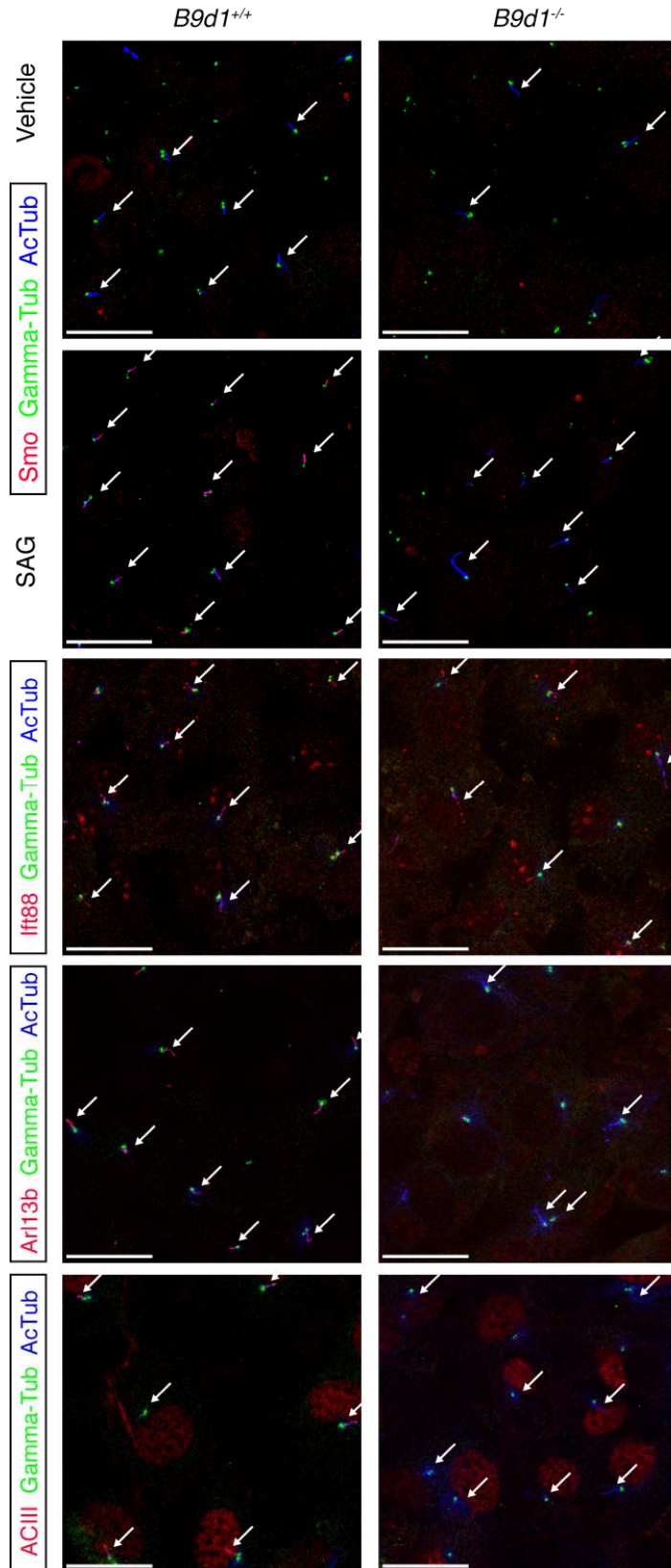
Figure S6. Protein localization in MEF cilia. Full panel view of protein localization depicted in Figures 4B and 4E-G. Arrows point to cilia. Scale bars, 25μm.
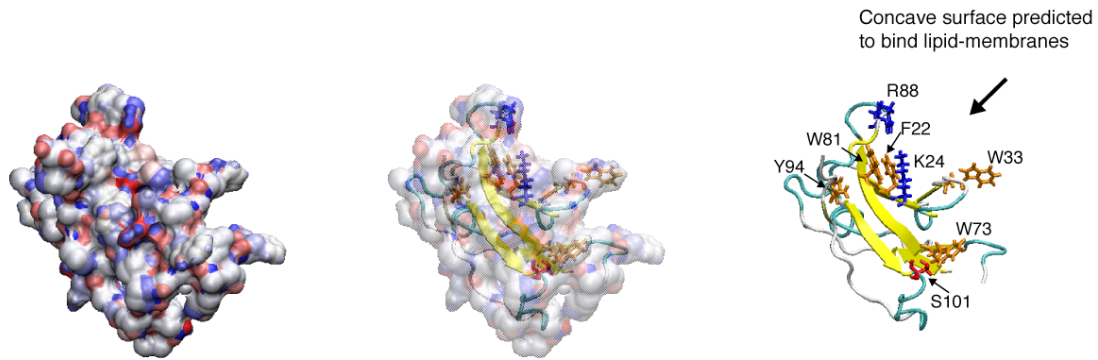
Figure S7. Modeling of B9D2 C2 domain. Electrostatic surface and cartoon modeling of the human B9D2 domain based on the structure of the calcium-free piccolo C2a domain. Electrostatic potential is colored in surface diagrams with positively charged residues colored in blue, and negatively charged residues in red. Conserved residues involved in membrane lipid binding are highlighted in licorice drawing with basic residues (K and R) in blue, aromatic residues (F, W and Y) in orange, and Ser101 in red. Residues 3-121 of human B9D2 were modeled, β-sheets are shown in yellow, and α-helixes are not shown.
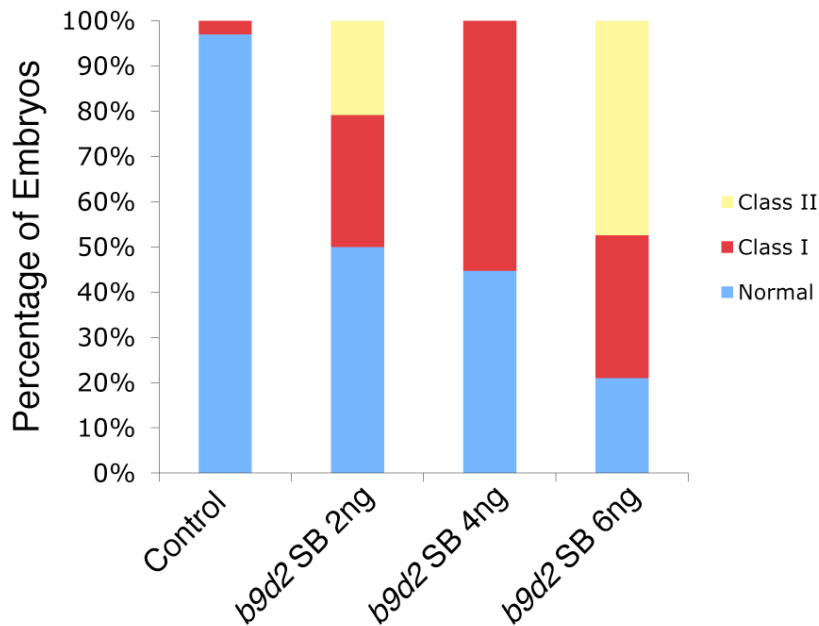

Figure S8. Titration curve of *b9d2* MOs. Injection of a *b9d2* splice blocker MO at concentrations of 0ng, 2ng, 4ng, and 6ng resulted in an increase in the number of embryos with early developmental defects (3%, 50%, 55% and 79%, respectively). A concentration of 2ng was used for all subsequent MO experiments.

Table S1. Scoring of the missense B9D2 mutation c.301A>C (p.Ser101Arg) by bioinformatic algorithms

Mutation	GD[1]		SIFT[2]		Align GVGD[3]		Mutation Taster[4]		Consensus
	VS	MG	VS	MG	VS	MG	VS	MG	MG
p.Ser101Arg	109	HLP	0.06	I	C65	HLP	0.99	HLP	LP

VS, Variant score; MG, Mutation Group; HLP, highly likely pathogenic; LP, likely pathogenic; I, indeterminate; N, neutral.

[1]GD (**G**rantham **D**istance): Measurement of chemical differences between the two amino acids under consideration.
[2]SIFT (**S**orting **I**ntolerant **F**rom **T**olerant): Multisequence alignment of orthologs.
[3]AlignGVGD: Multisequence alignment of orthologs.
[4]Mutation Taster (Schwarz JM et al.: Mutation Taster evaluates disease-causing potential of sequence alterations. Nat Methods 7: 575-6, 2010).

Interpretation of variant scores (VS) and deduced mutation group (MG):
Grantham distance: The Grantham score for chemical differences is a measurement for chemical differences between amino acids that combines residue side chain composition, polarity and volume. Similar pairs of amino acids score in the range of 5 to 60, whereas strongly dissimilar pairs score>100 (Grantham, 1974).
SIFT: 0.0 (HLP), 0.01-0.04 (LP), 0.05-0.09 (I), >0.1 (N).
AlignGVGD: C55-C65 (HLP), C35-45 (LP), C15-25 (I), C00 (N).
Mutation Taster: Predicted to be disease causing; the p value is the probability of the prediction, i.e. a value close to 1 indicates a high 'security' of the prediction. Please note that the p value used here is not the probability of error as used in t-test statistics.

Table S2. Primer sequences

Application	Name	Sequence
qRT-PCR	Ptc1F	5'-TGATTGTGGAAGCCACAGAAAA-3'
qRT-PCR	Ptc1R	5'-TGTCTGGAGTCCGGATGGA-3'
qRT-PCR	Gli1F	5'-CTTCACCCTGCCATGAAACT-3'
qRT-PCR	Gli1R	5'-TCCAGCTGAGTGTTGTCCAG-3'
qRT-PCR	β-actinF	5'-CACAGCTTCTTTGCAGCTCCTT-3'
qRT-PCR	β-actinR	5'-CGTCATCCATGGCGAACTG-3'
RT-PCR	B9d1Ex1F	5'-AAGACAACCGAGAGCCTCCT-3'
RT-PCR	B9d1Ex2R	5'-CAGTCCTGGCCATACACAAA-3'
RT-PCR	B9d1Ex3Ex4F	5'-GGCTGGCCACAGATTGTACT-3'
RT-PCR	B9d1Ex7R	5'-TCCTTGGTCACCACATTGAA-3'
Microsatellite analysis	ComF	5'-TACGCATCCCAGTTTGAGACG-3'
B9D2 sequencing exon 1	1F	5'-TTTGCCGTAGCTGGAGAGAC-3'
B9D2 sequencing exon 1	1R	5'-CCCCAGCAAGCTCCATAAG-3'
B9D2 sequencing exon 2	2F	5'-CATGGGTTGGCAATTAGGA-3'
B9D2 sequencing exon 2	2R	5'-CTGGGCCTGGAGTACTGAGA-3'
B9D2 sequencing exon 3	3F	5'-GGTTCCAGAGTCCATGCTTC-3'
B9D2 sequencing exon 3	3R	5'-CAGGGACAGGTCTTGGTGTT-3'
B9D2 sequencing exon 4	4F	5'-CCTGGGGTCTCCAGTGAGTA-3'
B9D2 sequencing exon 4	4R	5'-GACCCCGAGGTCCTAGAAAG-3'